ENHANCED BACKSCATTERING FROM RANDOMLY DISTRIBUTED SPHERICAL SCATTERERS AT 30 GHZ: COMPUTER SIMULATION AND COMPARISON WITH MEASUREMENT

Tomohiro Oguchi[1)] and Toshio Ihara[2)]
1)Institute of Science and Technology, Kanto Gakuin University
2) Dept. of Electrical, Electronic and Information Engineering, Kanto Gakuin University
1-50-1 Mutsuura-Higashi, Kanazawa-ku, Yokohama, Kanagawa 236-8501, Japan
ihara@kanto-gakuin.ac.jp

1. Introduction

The enhanced backscattering from random discrete scatterers has been intensively studied in various branches of physics. In the theoretical treatment, a second-order theory, with a plane-wave incidence, has been commonly used [1],[2], and the theory has been recently extended to the case of finite beamwidth [3]. Computer simulations of the problem have been mostly based on Monte Carlo technique, and the technique has been successfully applied to show vector character of light in enhanced backscattering from a plane-parallel medium containing Rayleigh scatterers [4].

To examine the multiple scattering effects in detail, we have conducted laboratory measurements of radar signatures of large water scatterers at 30 GHz under controlled scattering environment [5], and confirmed the effect of backscattering enhancement by using a mirror-image technique [6]. We have also conducted a computer simulation of the enhanced backscattering, assuming the same condition as in our measurements. The present paper reports on the computer simulation and comparison with the laboratory measurements.

2. Simulation Model and Problem Formulation

In view of the finiteness in scattering volume size, we directly evaluated the multiply scattered waves of nth order from all the scatterers by constructing n-particle scattering channels within the scattering volume.

When a transmitted wave travels through n successive scattering centers ($n \geqq 2$) in a scattering medium from scatterer 1 to scatterer n and enters into a receiver, another

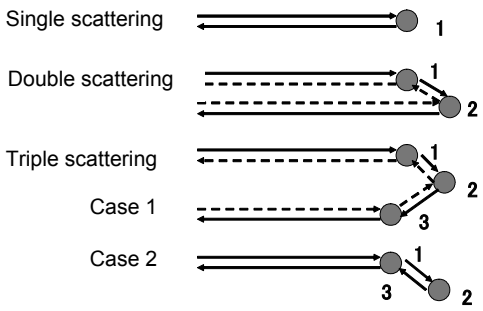

Fig. 1. Schematic diagram of scattering process.

wave also exists in the medium that travels in the opposite direction from scatterer n to scatterer 1 (time-reversed path) exactly on the same channel, as shown by the dashed lines in Fig. 1.

If the transmitting (TX) and receiving (RX) antennas are in the same position, these two waves will be added in phase resulting in enhanced backscattering. In triple scattering, however, there is the case that scatterer 3 is scatterer 1 itself as "Case 2" in Fig.1. In this case, the time-reversed path will not exist. In quadruple or higher-order scattering, the scattering path becomes much more complicated.

Fig. 2 shows the geometry and the symbols used in the following equations. While the TX

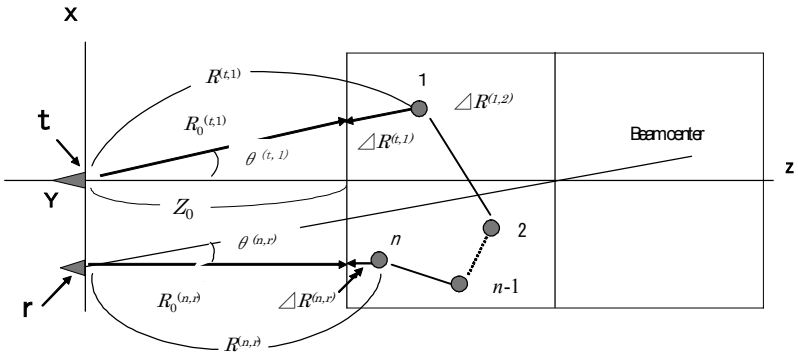

Fig.2. Geometry and symbols used in the computer simulation.

ISBN: 89-86522-78-0 94460©KEES

antenna (**t**) with its beam center along Z axis was fixed at the origin of a Cartesian coordinate system (X, Y, Z), the RX antenna (**r**) was able to move along X axis on Z = 0 plane, always pointing its beam center to the center of the rectangular scattering volume. The scattering volume was made of two cubic styrofoam blocks, each containing 868 spherical scatterers, and was extending from $Z = z_0$ toward the positive Z direction. (The total number of scatterers was thus 1736.)

The interaction of the waves will be written as follows. Let the electric fields of horizontally and vertically polarized wave, E_h and E_v, be expressed by a two-dimensional vector

$$\mathbf{E} = \begin{bmatrix} E_h \\ E_v \end{bmatrix} \tag{1}$$

We then define the four-dimensional vector **D** by

$$\mathbf{D} = \mathbf{E} \otimes \mathbf{E}^* \tag{2}$$

where $\otimes$ denotes the Kronecker product.

Letting $\mathbf{E}^{(1,n)}$, $\mathbf{E}^{(n,1)}$ be the received electric fields after the successive scattering from scatterer 1 to scatterer n, and scatterer n to scatterer 1, respectively, **D** may be written as

$$\begin{aligned}\mathbf{D} &= (\mathbf{E}^{(1,n)} + \mathbf{E}^{(n,1)}) \otimes (\mathbf{E}^{(1,n)^*} + \mathbf{E}^{(n,1)^*}) \\ &= (\mathbf{E}^{(1,n)} \otimes \mathbf{E}^{(1,n)^*} + \mathbf{E}^{(n,1)} \otimes \mathbf{E}^{(n,1)^*}) \\ &\quad + (\mathbf{E}^{(1,n)} \otimes \mathbf{E}^{(n,1)^*} + \mathbf{E}^{(n,1)} \otimes \mathbf{E}^{(1,n)^*})\end{aligned} \tag{3}$$

where the terms in the upper and lower parentheses in the last equation correspond to the ladder and cyclical terms in the diagrammatical theory.

Letting $\mathbf{E}^0$ be the effective electric-field vector of unit amplitude at the input-port of TX antenna, $\mathbf{E}^{(1,n)}$ and $\mathbf{E}^{(n,1)}$ may be expressed by

$$\begin{aligned}\mathbf{E}^{(1,n)} &= T(t,1:n,r)\,\mathbf{S}^{(1,n)}\mathbf{E}^0 \\ \mathbf{E}^{(n,1)} &= T(t,n:1,r)\,\mathbf{S}^{(n,1)}\mathbf{E}^0\end{aligned} \tag{4}$$

where

$$T(t,1:n,r) = C\left\{\frac{\exp\left[-ik(R_0^{(t,1)} + R_0^{(n,r)})\right]}{R^{(t,1)}R^{(n,r)}}\right\}$$

$$\exp\left[-ik_e(\Delta R^{(t,1)} + \Delta R^{(n,r)})\right]$$

$$\prod_{i=1}^{n-1}\left\{\frac{\exp(-ik_e\Delta R^{(i,i+1)})}{\Delta R^{(i,i+1)}}\right\} F_e^{(t,1)} F_e^{(n,r)}. \tag{5}$$

$T(t,n{:}1,r)$ is given by replacing 1 by n, and n by 1. In equation (5), k is the propagation constant in free space, k_e is the effective propagation constant in the scattering volume, and C is a constant factor given by

$$C = \frac{\lambda}{4\pi}\sqrt{2\eta P_t G_{t0} G_{r0}} \tag{6}$$

where λ is the wavelength, η is the characteristic impedance in free space, P_t is the TX power, G_{t0} and G_{r0} are the gains of TX and RX antennas in the direction of beam center, respectively, $F_e^{(i,j)}$ is the field directivity function of an antenna with a half-power beamwidth θ_b, when looking at a direction making an angle $\theta^{(i,j)}$ with its beam center

$$F_e^{(i,j)} = \exp\left[-2\left(\frac{\theta^{(i,j)}}{\theta_b}\right)^2 \log_e 2\right] \tag{7}$$

and for n = 1, we set

$$\prod_{i=1}^{n-1}\{\cdots\} = 1 \tag{8}$$

$\mathbf{S}^{(1,n)}$ and $\mathbf{S}^{(n,1)}$ are the product of n scattering matrices of the scatterers comprised in a specific path and its time-reversed path, respectively,

$$\begin{aligned}\mathbf{S}^{(1,n)} &= \mathbf{S}^{(n)}\mathbf{S}^{(n-1)}\cdots\mathbf{S}^{(2)}\mathbf{S}^{(1)} \\ \mathbf{S}^{(n,1)} &= \overline{\mathbf{S}}^{(1)}\overline{\mathbf{S}}^{(2)}\cdots\overline{\mathbf{S}}^{(n-1)}\overline{\mathbf{S}}^{(n)}\end{aligned} \tag{9}$$

where the overbars denote that the matrices are those in time-reversed path.

For any number of successive scatterings, the reciprocity relation exists for the matrices $\mathbf{S}^{(1,n)}$ and $\mathbf{S}^{(n,1)}$ [7]

$$\mathbf{S}^{(n,1)} = \mathbf{Q}\mathbf{S}^{(1,n)^{\mathrm{T}}}\mathbf{Q} \tag{10}$$

where $\mathbf{Q} = diag(-1,1)$. Using the local right handed coordinate system always looking at the wave propagation direction, Eq. (3) is expressed by

$$\begin{aligned}\mathbf{D} = [&T(t,1:n,r)T(t,1:n,r)^*\mathbf{S}^{(1,n)} \otimes \mathbf{S}^{(1,n)^*} \\ &+ T(t,n:1,r)T(t,n:1,r)^*\mathbf{Q}\mathbf{S}^{(1,n)^{\mathrm{T}}}\mathbf{Q} \otimes \\ &\quad \mathbf{Q}\mathbf{S}^{(1,n)^{\mathrm{T}}{}^*}\mathbf{Q}](\mathbf{E}^0 \otimes \mathbf{E}^{0^*}) \\ &+ [T(t,1:n,r)T(t,n:1,r)^*\mathbf{S}^{(1,n)} \otimes \mathbf{Q}\mathbf{S}^{(1,n)^{\mathrm{T}}{}^*}\mathbf{Q} \\ &+ T(t,n:1,r)T(t,1:n,r)^*\mathbf{Q}\mathbf{S}^{(1,n)^{\mathrm{T}}}\mathbf{Q} \otimes \\ &\quad \mathbf{S}^{(1,n)^*}](\mathbf{E}^0 \otimes \mathbf{E}^{0^*}).\end{aligned} \tag{11}$$

Excluding the case that the TX and RX antennas are in the same position, the scattering matrices of the scatterers 1 and n directly facing to the antennas do not exactly satisfy the reciprocity relation. We, however, assume that Eq. (10) is always satisfied, since the distance between these two antennas is normally very small.

3. Computational Procedure of Numerical Simulations

The major parameters used in the numerical simulation are given in Table 1. While the scatterers were water-injected thin polystyrene spheres of radius 12.5 mm, we assumed that, as in our preceding work [5], their scattering properties are the same as those of water spheres of radius 12.5 mm.

In our simulation, random numbers were generated to give three-dimensionally randomized positions of the scatterers. The minimum intercentral distance between scatterers was kept above 6 times the wavelength, since a careful examination showed that the far-field approximation could safely be used above that distance.

We evaluated the double scattering for each combination of scatterer positions in equation (11) with $n = 2$, and the results were added for all the combinations of scatterer positions. We then repeatedly executed the computations for differently randomized positionings of scatterers 32 times, and averaged the values. This average was adopted as the received power for double scattering. The number of averaging (32 times) was the maximum attainable number in our measurements [5].

With the increasing order of scattering, the number of scattering paths increases almost exponentially. For our scatterer number of 1736, the computation time exceeds acceptable level for triple scattering and higher. For those cases, the scattering paths were sampled to reduce the computation time. Then we estimated the scattered power of the total paths from the scattered power of the sampled paths by a proportional allotment according to the numbers of the total paths and sampled paths. Our examination on the accuracy of the estimate has justified the sampling approach. We have ignored the effect of the specific path in which some scatterer is involved in a scattering channel more than once in quadruple scattering or higher. In triple scattering, however, calculations were made for both total and sampled paths, taking account of the specific paths. The final received power was the sum of the value for each order of scattering. Since the results for different order of scattering might be not correlated, we added the results independently. Further, we have ignored the product of the fields of different scattering channels because of their random nature.

Table 1 Major parameters of numerical simulation

Frequency	30 GHz
Size of the scattering volume	0.9 m × 0.9 m × 0.9 m
Scatterers	
Size in radius	12.5 mm
Number	1736 (868 × 2)
Distance from the transmitter to the front face of scattering volume	3.15 m
Transmitting and receiving antennas	
Beamwidth	10 degrees
Gain	25 dBi
Transmitting power	0 dBm
Scattering angles adopted in the calculation	0 (exact backscattering), 0.2, 0.4, 0.6, 0.8, 1.0, 2.0, 3.0 degrees

4. Simulation Results

Fig. 3 shows the relation between co-polar received powers and scattering angles, calculated for both single and double scatterings. Vertically polarized incident wave is assumed. (Electric field vector is in the direction of Y axis.) The symbols l and c signify ladder and cyclical terms, respectively. In the double scattering, the enhancement is certainly seen at around an angle of 0°. Although not shown here, this effect is more pronounced in the cross-polar channel. If the TX and RX antennas have the same directivity, the ladder and cyclical terms have the same value at an angle of 0° in both co-polar and cross-polar channels

Fig. 4 shows the calculation result for triple scattering for total and sampled paths. The overall effect of the sampling of scattering paths seems not to produce significant error. The value of cyclical term for an angle of 0° is slightly smaller than that of ladder term because of the

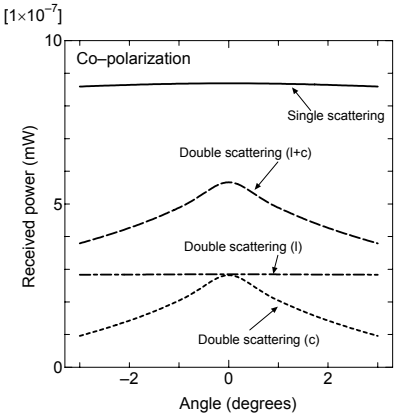

Fig. 3. Single and double scattering received powers versus scattering angle.

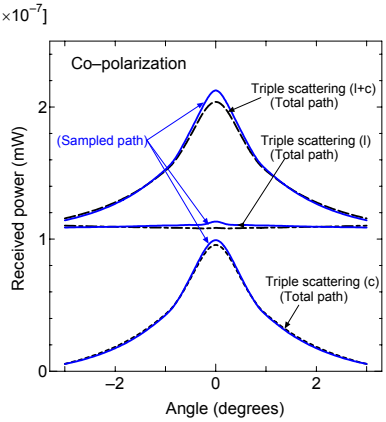

Fig. 4. Triple scattering received power versus scattering angle.

effect of some specific path where some scatterer is involved twice.

Figs. 5 (a) and (b) illustrate the total scattered powers obtained by summing up to septuple scattering for co- and cross-polar channels, respectively. The numerical convergence of the values is confirmed by a separate examination, although not shown here. It is suggested that the angular range of enhancement is of the order of a wavelength divided by the mean free path of scattering [1]. The estimate for the present case is about 0.8degrees, in fairly good agreement with the simulation curve.

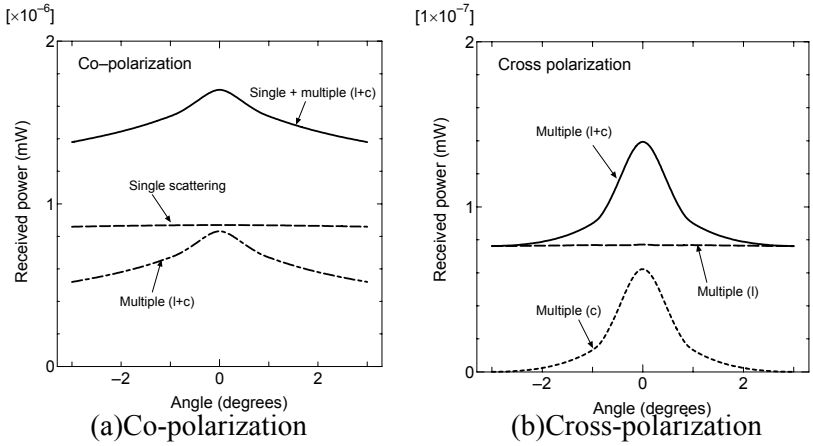

(a)Co-polarization (b)Cross-polarization

Fig. 5. Total received powers (sum of the single to septuple scattering) versus scattering angle.

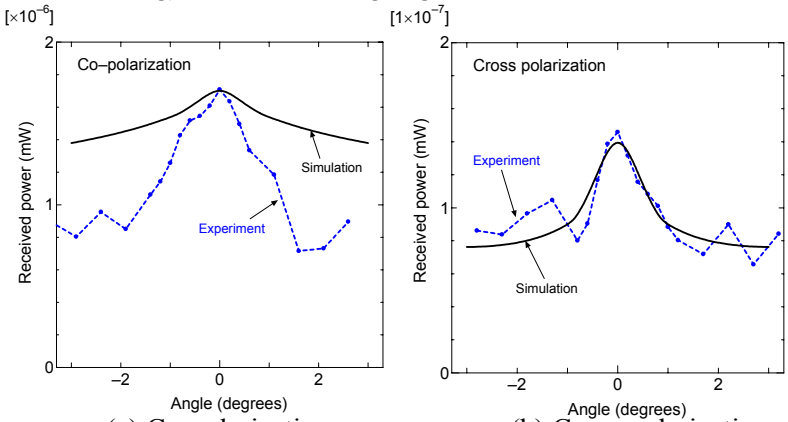

(a) Co-polarization (b) Cross-polarization

Fig. 6. Comparison of calculated received powers with measurements.

5. Comparison with Measurements

Figs. 6 (a) and (b) compare the simulated values with measurements [6] for co- and cross-polar channels, respectively. The simulated co- and cross-polar received powers are the same as those labeled by "single + multiple (l + c)" and "multiple (l + c)" in Fig. 5, respectively. The calculated peak value of co-polar received power was –57.67 dBm, while the calibrated measured value was –56.0 dBm. In view of unavoidable experimental errors, the agreement seems to be satisfactory. To obtain better fit, however, the measured co-polar curve was shifted vertically, and to some extent horizontally: A very small horizontal shift was needed to compensate for an error in angles. The cross-polar values were also shifted in the same way so as to keep the relative difference unchanged between the co- and cross-polar values. The measured relative magnitude of co- and cross-polar received powers is in good agreement with the calculated ones. The sharpness of the cross-polarized curves agrees fairly well, although the agreement is poor in co-polar case.

6. Conclusions

A computer simulation of backscattering enhancement has been made by adopting a simple direct-simulation method, and several of knowledge on the detailed characteristics of enhanced backscattering have been obtained. It was also found that the relative magnitude of co- and cross-polar received powers agrees fairly well between the calculation and measurement. The agreement, however, is poor for the curves' sharpness in co-polar case, while there is a fairly good agreement in cross-polar case.

References

[1] Kuga, Y., L. Tsang, and A. Ishimaru, *JOSA Communications*, *2*(4), pp.616-618 (1985).

[2] Mandt, C. E., L. Tsang, and A. Ishimaru (1990), *J. Opt. Soc. Am. A*, *7*(4), pp.585-592 (1990).

[3] Kobayashi, S. et al., *Proc. SPIE Fourth International Asia-Pacific Environmental Remote Sensing Symposium*, 5654-13, Honolulu, Hawaii, USA. Nov (2004).

[4] van Albada, M. P., and A. Lagendijk, *Physical Review B*, 36(4), pp.2353-2356 (1987).

[5] Tazaki, T. et al., *IEE Proc.-Mocrow. Antennas Propag.*, *147*(1), pp.8-12 (2000).

[6] Ihara, T., T. Oguchi, and T. Tazaki, *Proc. URSI Commission F Open Symposium*, pp.59-64, Cairns, Australia, June (2004).

[7] Mishchenko, M. I., *J. Opt. Soc. Am. A*, *9*(6), pp.978-982 (1992).